J. Fluid Mech. (1978), *vol.* 85, *part* 1, *pp.* 33–56
Printed in Great Britain

Wall region of a relaxing three-dimensional incompressible turbulent boundary layer

By K. S. HEBBAR
Aerodynamics Division, National Aeronautical Laboratory, Bangalore 560017, India

AND W. L. MELNIK
Department of Aerospace Engineering, University of Maryland, College Park

(Received 14 February 1977)

An experimental investigation was conducted at selected locations in the wall region of a three-dimensional turbulent boundary layer relaxing in a nominally zero external pressure gradient behind a transverse hump (in the form of a 30° swept, 5 ft chord, wing-type model) faired into the side wall of a low-speed wind tunnel. The boundary layer (approximately 3·5 in. thick near the first survey station, where the length Reynolds number was $5{\cdot}5 \times 10^6$) had a maximum cross-flow velocity ratio of 0·145 and a maximum cross-flow angle of 21·9° close to the wall. The hot-wire data indicated that the apparent dimensionless velocity profiles in the viscous sublayer are universal and that the wall influence on the hot wire is negligible beyond $y^+ = 5$. The existence of wall similarity in the relaxing flow field was confirmed in the form of a log law based on the resultant mean velocity and resultant friction velocity (obtained from the measured skin friction).

The smallest collateral region extended from the point nearest to the wall ($y^+ \approx 1$) up to $y^+ = 9{\cdot}7$, corresponding to a resultant mean velocity ratio (local to free-stream) of 0·187. The unusual feature of these profiles was the presence of a narrow region of slightly decreasing cross-flow angle (1° or less) that extended from the point of maximum cross-flow angle down to the outer limit of the collateral region. A sublayer analysis of the flow field using the measured local transverse pressure gradient slightly overestimated the decrease in cross-flow angle. It is concluded that, in the absence of these gradients, the skewing of the flow could have been much more pronounced practically down to the wall (limited only by the resolution of the sensor), implying a near-wall *non-collateral* flow field consistent with the equations of motion in the neighbourhood of the wall.

The streamwise relaxation of the mean flow field based on the decay of the cross-flow angle was much faster in the inner layer than in the outer layer. Over the streamwise distance covered, the mean flow in the inner layer and the wall shear-stress vector relaxed to a two-dimensional state in approximately 10 boundary-layer thicknesses whereas the relaxation of the turbulence was slower and was not complete over the same distance.

1. Introduction

Despite the fact that three-dimensional turbulent boundary layers are of great practical interest because of their wide occurrence in nature, it is only in recent years

that interest in their study has begun to grow steadily The analysis of three-dimensional turbulent boundary layers is in a state of flux compared with the analysis of two-dimensional problems (Nash & Patel 1972, p. 4). On the experimental side, very few detailed studies of the three-dimensional problem have been published. Most theoretical approaches to the solution of a two-dimensional turbulent boundary layer depend on experimental data to model the shear-stress distribution (i.e. to model the closure equation). With three-dimensional flows, the data must in addition provide information on the directional characteristics of the flow, i.e. the distributions of the shear-stress vector and the mean velocity vector across the boundary layer. The prediction methods at present available (Mellor 1967; Nash 1969; Bradshaw 1971; Cebeci 1974, 1975) show some success in treating the incompressible three-dimensional turbulent boundary layer. Wheeler & Johnston (1973) have made a critical assessment of some of these methods. Common to all of these calculation techniques is the need for complete and detailed experimental data to evaluate existing theoretical models and to develop more adequate models for the fluctuation terms in the time-averaged equations for the mean motion (Bradshaw 1969).

A number of experimental investigations on three-dimensional turbulent boundary layers have been reported to date (Johnston 1960, 1970; Bradshaw & Terrell 1969; Hornung & Joubert 1963; East & Hoxey 1969; Rogers & Head 1969; Klinksiek & Pierce 1970; Bissonnette 1974; Vermeulen 1971; Prahlad 1968, 1973; Swamy 1971; Etheridge 1972; Power 1973; van den Berg *et al.* 1975). In many of these experiments (Johnston 1960, 1970; Hornung & Joubert 1963; East & Hoxey 1969; Prahlad 1968), pressure gradients dominate the mean flow field and therefore they cannot be considered as adequate test cases to provide meaningful data for studying and improving the assumptions made in turbulence models for the distribution of shear stress. The question of the correlation between the directions of the shear-stress vector and the mean velocity-gradient vector still remains unresolved. Another unresolved question concerns the nature of the mean flow field very close to the wall. Most of the existing data indicate collateral near-wall flow, i.e. in the inner region very close to the wall (often extending to ratios of local to free-stream velocity as high as 0·5) the mean velocity vector does not change its direction. More (reliable) data are still needed to resolve experimentally the existence (or non-existence) of a collateral near-wall flow field in a three-dimensional turbulent boundary layer. This is all the more important because the existence of such a collateral flow field is not predicted either by numerical calculations (East & Pierce 1972; Pierce & East 1972) or by a sublayer analysis of the flow field (Nash & Patel 1972, p. 102).

The original aim of the present investigation was to find experimental answers to the aforementioned questions. As strongly advocated by Bradshaw (1969), a satisfactory test case is the flow past an infinite swept wing (Bradshaw & Terrell 1969), where the mean-flow development is primarily influenced by the shear-stress gradients. The experimental configuration of flow geometry and flow conditions studied in this investigation was selected to approximate this test case on a large scale (but with a low aspect ratio wing). A traverse mechanism specially designed for near-surface anemometer studies enabled an investigation of the near-wall region of the relaxing boundary layer at selected locations. The experiments included near-wall measurements of the time-mean and fluctuating velocity in planes parallel to the wall with a single rotated hot-wire probe and measurements of the wall shear stress with various

shear-stress devices (a flush-mounted hot-film gauge, a sublayer fence and two Preston probes). A detailed account of the present investigation may be found in Hebbar (1976) and Hebbar & Melnik (1976).

2. Flow configuration and instrumentation

The details of the University of Maryland Boundary Layer Research Tunnel used in the present investigation are given in Hebbar (1976). It is essentially a low-speed indraft-type open-circuit tunnel with a 20 ft long closed test section of nominal cross-section 18 in. wide by 46·5 in. high (figure 1). To facilitate the spatial resolution of the measurements, a relatively thick two-dimensional turbulent boundary layer was first developed on the side wall of the tunnel over a run length of about 12 ft and then allowed to flow over a transverse hump faired into the side wall. The hump was in the form of a 30° swept, approximately 8 % thick (symmetric), 5 ft chord, wing-type model that spanned the tunnel height. Its trailing-edge thickness was estimated to be 0·0002 in. The boundary layer downstream of the hump relaxed under a nominally zero external pressure gradient and eventually returned to a two-dimensional state. The measurements were made downstream of the hump, where the flow configuration was similar to the flow field in the experimental study of Bradshaw & Terrell (1969), the boundary layer being about three times as thick with nearly three times the induced-wall cross-flow.

The random fluctuations in the free-stream velocity in the test section were within $\pm 0{\cdot}3$ % (as observed on a micromanometer). The two-dimensional longitudinal wall static pressure distribution in the test section (in the absence of the hump) indicated a very small favourable pressure gradient (less than 0·3 % of the upstream reference dynamic head per foot). The longitudinal intensity of free-stream turbulence in the test section (in the absence of the hump) was 0·2 % at a free-stream velocity of 50 ft/s.

A well-polished aluminium plate $\frac{1}{4}$ in. thick and 8 ft long epoxied to the end of the rear wall of the test section provided a smooth working surface (test wall). In all, the test wall contained 10 instrumentation ports and 77 static taps (figure 2). When not in use, each port was closed with a custom-fitted plug having a static tap at its centre.

In the experimental investigation the following measurements were made in the relaxing region:

(i) measurements of the time-mean and fluctuating velocity vector in the near-wall region with a single rotated hot wire;

(ii) measurements of the time-mean wall shear-stress vector with a flush-mounted hot-film gauge, a sublayer fence and two Preston probes;

(iii) measurements of the local free-stream velocity with a conventional Pitot–static probe;

(iv) measurements of the wall static pressure.

The traverse mechanism was mounted externally on the test wall so that a probe could be introduced through the working surface (figure 1). This arrangement facilitated hot-wire measurements as close as 0·0005 in. from the wall with minimum interference. The traverse mechanism is essentially a development of the hot-wire probe of Wills (1967) and is similar to that of Rogers & Head (1969) in principle and operation but differs in constructional details. It has a travel distance of 1 in. with a resolution of 0·0001 in. A rotation of 140° with a resolution of 1′ is possible. A detailed description of

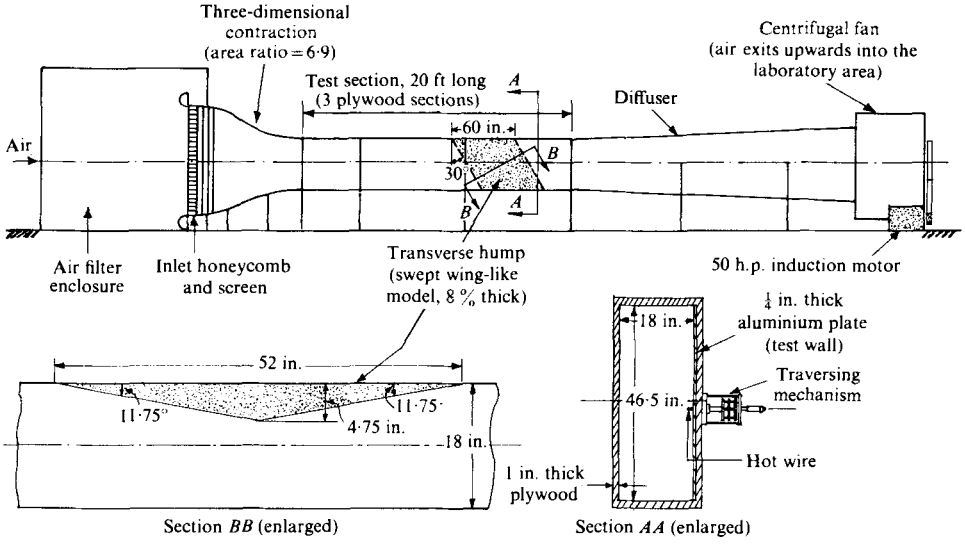

FIGURE 1. Boundary-layer research tunnel and flow geometry.

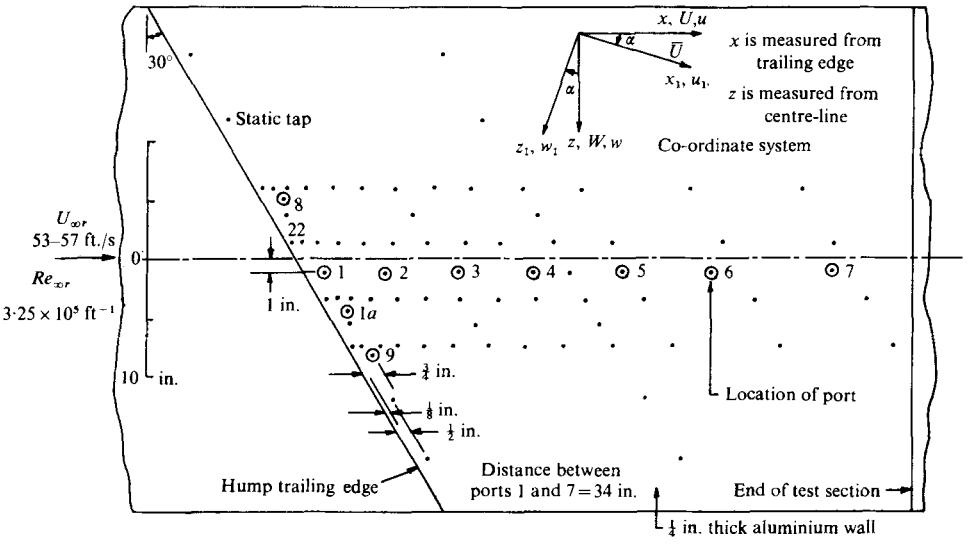

FIGURE 2. Location of instrumentation ports and static taps.

the traverse mechanism, its mounting and its initial orientation is given in Hebbar (1976). The hot-wire sensor consisted of a central sensitive section of platinum-coated tungsten wire 3·8 μm (0·00015 in.) in diameter and 1·25 mm (0·050 in.) long with approximately 0·001 in. diameter copper-plated end sections† soldered to the tips of two sewing needles mounted $\frac{1}{8}$ in. apart in a probe holder. Each of the hot wires used in the present investigation had a length-to-diameter ratio of 333·3 and a nominal sensor resistance of 6 Ω (at 25 °C). The combined resistance of the needles and the

† Obtainable as a replacement sensor in cards of 12 wires from Thermo-Systems, Inc., 2500 North Cleveland Avenue, St Paul, Minnesota 55113.

electrical leads was nominally 0·47 Ω (at 25 °C). The hot wires were operated from a DISA 55D01 constant-temperature anemometer unit at a resistance of usually 1·8 times the cold resistance.

The hot-film gauge consisted of a thin platinum film deposited at the centre of a Pyrex disk. The sensitive portion of the film was 0·004 in. wide, 0·130 in. long and about 2000 Å thick and was coated with alumina (about 9500 Å thick). The hot film had an aspect ratio of 32·5 and a nominal film resistance of 14·025 Ω at 25 °C. The leads, each about 2 ft long, had a resistance of nearly 0·21 Ω. The usual operating resistance as set on the DISA 55D01 constant-temperature anemometer was 19·00 Ω, corresponding to a film temperature of 250 °C.

A sublayer fence was used to duplicate the measurements by the hot-film gauge so as to provide an independent check on the performance of the latter. The fence was 0·003 in. wide and 0·125 in. long and protruded 0·003 in. from the working face. The static pressure drop across the fence was sensed by two slots (each 0·003 in. wide and 0·125 in. long on either side of the fence). Finally Preston probes were used as overall checks on the performance of the hot-film gauge and the sublayer fence.

3. Experiments

All the measurements were made at a constant upstream reference Reynolds number of $3{\cdot}25 \times 10^5\,\mathrm{ft}^{-1}$, corresponding to a local free-stream velocity of 53–57 ft/s in the relaxing region. The upstream reference station was located at a distance of 5 ft from the beginning of the test section and port 1 nearly 12 ft downstream of the reference station. A standard Pitot–static probe permanently installed at the reference station was used to monitor the tunnel speed on a micromanometer. Before setting up the speed, the tunnel was allowed to run for some time to attain steady-state conditions.

Earlier measurements by Winkelmann (1976) had indicated a thickness of nearly 3·5 in. for the two-dimensional boundary layer. The hot-wire measurements made in this investigation were limited by the traverse mechanism to 0·95 in., so that each hot-wire survey covered the entire inner layer region and a small portion beyond it. The survey points (i.e. y values) across the boundary layer, excluding a region 0·010 in. wide within the viscous sublayer adjacent to the wall, were distributed in such a way that when plotted on a logarithmic scale their wall co-ordinates y^+ were very nearly equally spaced. Traversing was always done in one direction only, from the outermost position of the hot wire towards the test wall.

3.1. *Two-dimensional experiments*

Measurements were made in the two-dimensional turbulent boundary layer (in the absence of the hump). These experiments were performed to determine the angular response of the flush-mounted hot-film gauge and the sublayer fence. More important, the two-dimensional measurements provided the necessary data to estimate the wall-proximity correction for hot-wire readings very close to the wall (Hebbar 1976; Hebbar & Melnik 1976). These corrections were later used for the three-dimensional hot-wire data very close to the wall. The two-dimensional experiments were restricted to two locations (ports 1 and 7, figure 2). In the three-dimensional flow field port 1 corresponded to the first streamwise measuring station in the relaxing region and port 7 to the last station.

In the case of hot-wire surveys, the hot wire was calibrated in a free jet just before and just after each survey. When the drift was small ($< 3\%$), the calibration curve interpolated from the initial and final calibration curves was used for reducing the hot-wire survey data; otherwise the experiment was usually repeated in its entirety.

3.2. *Three-dimensional experiments*

Hot-wire surveys of the mean velocity vector required that the direction measurement preceded the magnitude measurement. All direction measurements were accomplished by the bisector method (Hebbar 1976). The aerodynamic symmetry of the probes (on whose accuracy the bisector method depended) was earlier verified by making a few directional measurements in the two-dimensional boundary layer. It was the usual practice to check the direction by repeating the experiment with a different angle between the sensor and the normal to the local mean direction of flow.

The wall static pressure distribution was measured with a micromanometer with tap 22 serving as the reference tap (figure 2). A separate run was made to measure the local free-stream velocity at each port location with a conventional Pitot–static probe of diameter 0·125 in. with an opening of 0·043 in. The probe tip was located at a distance of approximately 8 in. from the wall and 1·75 in. ahead of the centre of the port.

4. Discussion of results

The experimental data are briefly discussed below with particular emphasis on (i) the nature of the mean flow field very close to the wall and (ii) the streamwise relaxation characteristics of the flow field in the inner layer.

4.1. *Wall static pressure and free-stream velocity in the relaxing region*

The wall static pressure measured in the region behind the trailing edge of the hump indicates a small (less than 3 % of the upstream reference dynamic head per foot) favourable pressure gradient in the streamwise direction (figure 3). Cross-plots of the curves in figure 3 indicate a small (less than 3·5 % of the upstream reference dynamic head per foot) adverse pressure gradient in the spanwise direction, parallel to the trailing edge. At a position 0·75 in. from the trailing edge, corresponding to the spanwise location of the instrumentation ports, the measured spanwise pressure gradient is within 2 % of the upstream reference dynamic head per foot. The spanwise pressure gradient in the neighbourhood of the tunnel centre-line decreases with distance from the trailing edge and is practically zero at the last two port locations.

Since the pressure gradients amount to less than 1 % of the upstream reference dynamic head over a spanwise distance of one boundary-layer thickness (approximately 3·5 in., Winkelmann 1976), the relaxing region along the streamwise line of ports may be considered to be nominally in a zero pressure gradient for analysis of the flow field away from the wall. However, the presence of even small lateral pressure gradients will influence the cross-flow field very close to the wall.

Figure 4 shows the variation of the local free-stream velocity along the streamwise line of ports. The free-stream velocity is very nearly constant from approximately 2·5 boundary-layer thicknesses downstream of the trailing edge, whereas in the region close to the trailing edge the measurements indicate a free-stream adverse pressure gradient of approximately 2 % of the upstream reference dynamic head per foot (where

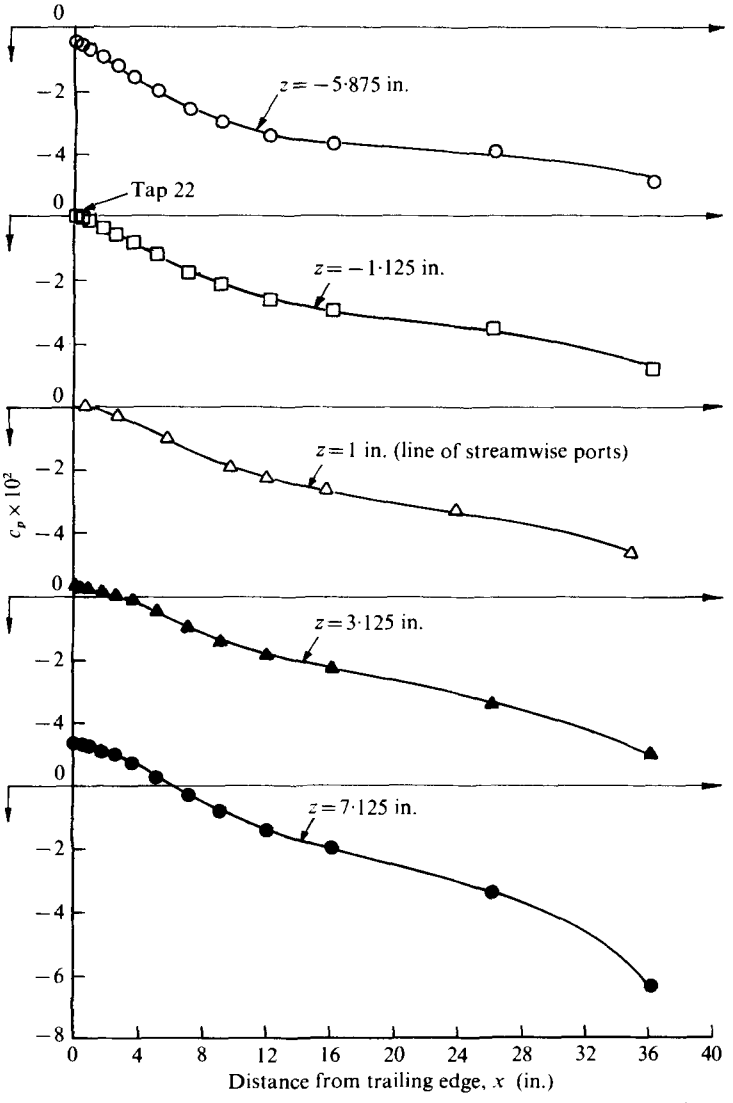

FIGURE 3. Streamwise wall static pressure distribution $c_p = (p - p_{tap\,22})/q_{\infty r}$ in the relaxing region, where $q_{\infty r}$ is the reference free-stream dynamic pressure. (Reference Reynolds number $Re_{\infty r} = 3{\cdot}25 \times 10^6$ to $3{\cdot}29 \times 10^5$ ft^{-1}.)

gradients in the free stream and on the wall differ in sign). However, in terms of the magnitude, both are small and the flow may be treated as having a nominally zero, external, streamwise pressure gradient.

4.2. *Direction profiles in the relaxing region*

The mean direction profiles (both measured and corrected) from hot-wire surveys are shown in figure 5. The resultant friction velocity $\overline{U}^*$ used in evaluating the wall co-ordinates was based on the resultant skin friction $\bar{c}_f$ determined from measurements by the 0·032 in. diameter Preston probe at the location in question. The hot-wire

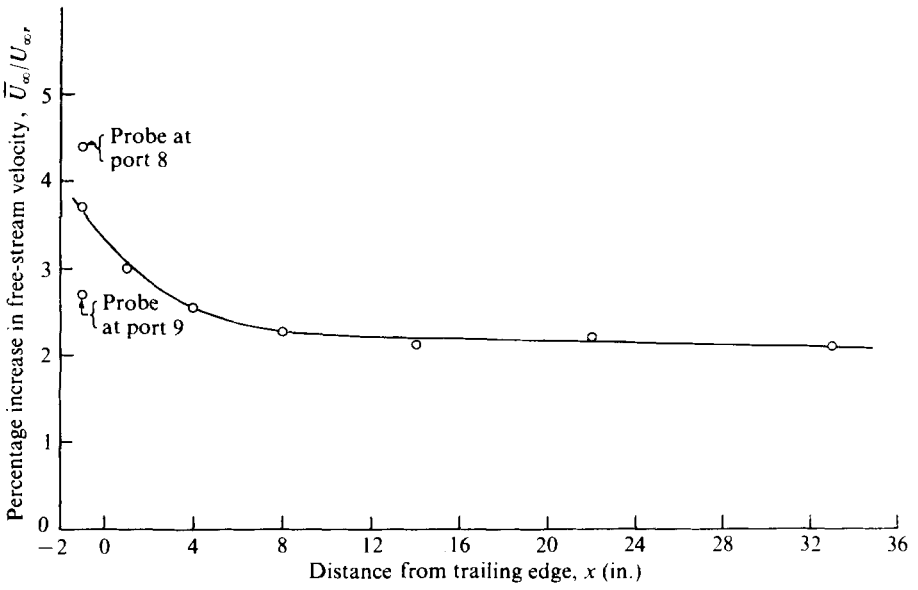

FIGURE 4. Variation of free-stream velocity in the relaxing region; nominal $Re_{\infty r} = 3{\cdot}25 \times 10^5$ ft^{-1}.

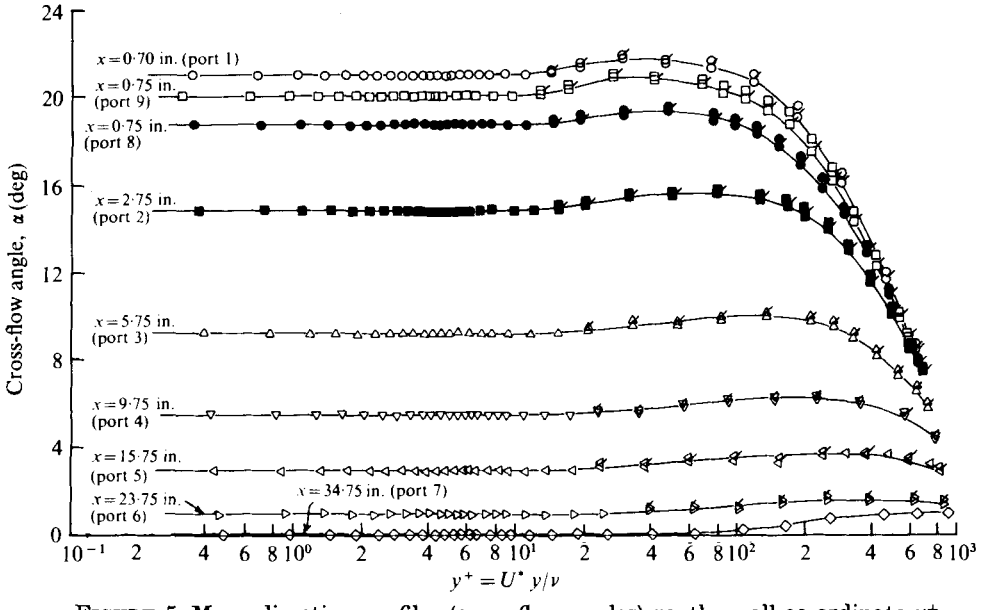

FIGURE 5. Mean direction profiles (cross-flow angles) *vs.* the wall co-ordinate y^+; nominal $Re_{\infty r} = 3{\cdot}25 \times 10^5$ ft^{-1}. Flagged symbols denote corrected data.

turbulence data were used for making angle corrections (Rose 1962; Hebbar 1976) to the indicated mean direction of flow to obtain the mean-flow direction (shown by flagged symbols). The angle correction, proportional to the velocity cross-correlation, is included here to show the effect of turbulence fluctuations on the mean angular response of the hot wire. However, in the present hot-wire surveys, the effect is small

(the maximum correction is less than 4 % of the measured value), therefore in subsequent discussions no distinction will be made between the mean direction of flow and the mean-flow direction.

The direction profiles indicate a small region of collateral flow (i.e. constant cross-flow angle) adjacent to the wall. With the exception of profiles at the last three survey stations, which are practically two-dimensional, the data indicate the existence of a collateral flow field up to $y^+ = 9{\cdot}7$–$17{\cdot}6$, y^+ increasing with $\overline{U}^*$. The value of y^+ at which the maximum cross-flow angle occurs in the inner layer varies from 27·1 to 144·8, y^+ increasing with $\overline{U}^*$ as before. The most striking feature in these profiles is the fact that the cross-flow angle decreases in a narrow region which extends from the point of maximum cross-flow down to the outer limit of the collateral region. Although the actual decrease in the cross-flow angle was small (of the order of 1° or less) it was observed consistently during the hot-wire surveys at all locations. In a three-dimensional boundary layer the cross-flow is driven by the spanwise components of the shear stress and impressed pressure field. Because of the presence of small transverse wall static pressure gradients (§ 4.1) opposing the cross-flow in the relaxing region, some decrease in the cross-flow angle should be expected as the wall is approached. A sublayer analysis of the flow field (§ 4.4) with the estimated values of the pressure gradients does indeed predict a decrease in the cross-flow angle close to the wall, the predicted decrease being slightly higher than the measured decrease.

4.3. *Mean velocity profiles in the relaxing region*

The resultant mean velocity profiles in the inner layer are shown in figure 6. The profile shapes close to the trailing edge resemble those in adverse-pressure-gradient flows and reflect the history of the boundary-layer development over the hump. The mean velocity distribution in the boundary layer relaxes and becomes fuller with distance from the trailing edge and at the last port location almost approaches the two-dimensional distribution obtained in the absence of the hump.

The experimental data shown in figure 7 indicate, in agreement with the earlier findings of Oka & Kostic (1972) and the present findings from the two-dimensional data (Hebbar 1976), that the apparent (measured) resultant velocity profiles in the viscous sublayer are universal (local) and that the wall influence on the hot wire is negligible beyond $y^+ = 5$. The scatter in the region $y^+ < 1{\cdot}5$ is largely due to errors in measuring very small distances from the wall. The universality of the apparent profiles justified the use of the wall-proximity correction curve suggested in Hebbar (1976) to correct the experimental data close to the wall ($y^+ < 5$). The corrected data are also shown (by flagged symbols) in figure 7. The agreement between the corrected data and the linear distribution $\overline{U}^+ = y^+$ is remarkable in the region $1{\cdot}5 < y^+ < 5$. The effect of correcting hot-wire readings for wall influence can be better appreciated from figure 8, where the corrected resultant mean velocity profiles close to the wall are shown in the usual co-ordinates and compared with the respective wall velocity gradient based on the resultant skin friction determined from Preston probe measurements. With the exception of the points closest to the wall (which could not be precisely located because of errors in measuring very small distances), the agreement between the corrected data and the respective wall velocity-gradient line is exceptionally good in the region of wall influence (which extends up to $y \simeq 0{\cdot}005$ in. at port 7 and $y \simeq 0{\cdot}008$ in. at port 9).

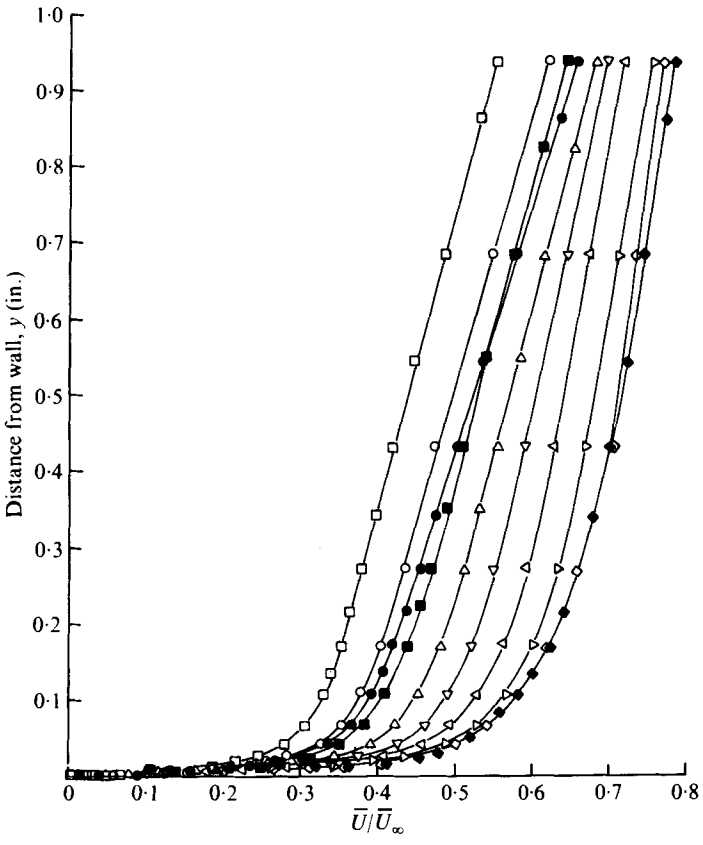

FIGURE 6. Resultant mean velocity profiles in the inner layer of the relaxing boundary layer; nominal $Re_{\infty r} = 3{\cdot}25 \times 10^5$ ft^{-1}.

	□	●	○	■	△	▽	◁	▷	◇	◆
x (in.)	0·75	0·75	0·75	2·75	5·75	9·75	15·75	23·75	34·75	34·75
Port	9	8	1	2	3	4	5	6	7	7 (two-dimensional)

Figures 9(*a*) and (*b*) show, in wall co-ordinates, the resultant mean velocity profiles in the inner layer of the relaxing region. For purposes of comparison, the log-law relation for the resultant velocity profile, with the constants suggested by Patel (1965), and the linear sublayer relation are shown in these figures. The existence of wall similarity in the relaxing region is confirmed by the mean velocity profiles, thus concurring with the findings of previous investigators for different flow configurations (Hornung & Joubert 1963; East & Hoxey 1969; Vermeulen 1971; Etheridge 1972; Prahlad 1968, 1973). The agreement of the data with the log-law relation is quite satisfactory at all but one location (port 9). It should be noted that a slight vertical shift of the log-law relation will bring it into closer agreement with the data at port 9.

The experimental mean velocity profiles at various port locations are presented in polar form in figures 10(*a*) and (*b*). Three vertical arrows labelled on each polar plot identify different locations in the boundary layer. The vast region between the outermost point ($U/\overline{U}_\infty = 1$, $W/\overline{U}_\infty = 0$) and the middle arrow represents the region of increasing cross-flow angle. The narrow region between the middle arrow and the

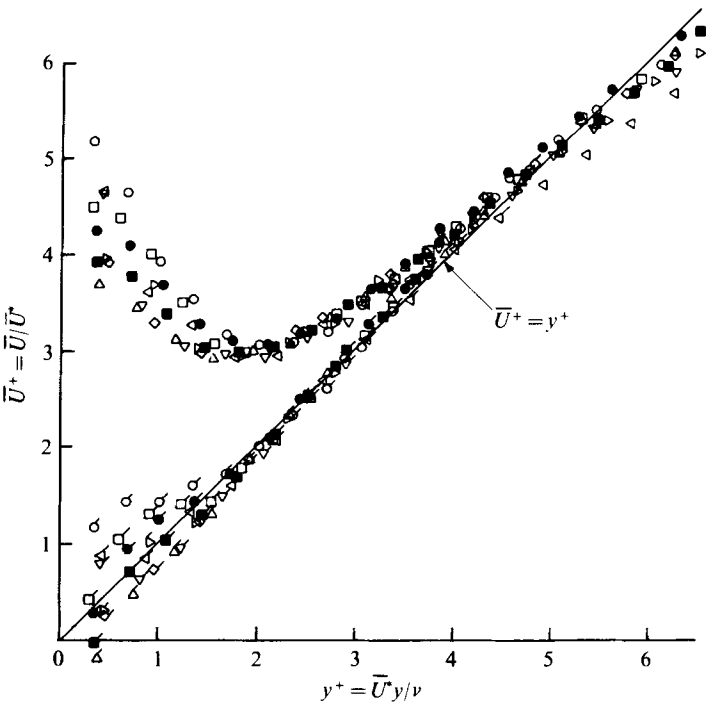

FIGURE 7. Resultant mean velocity profiles close to the wall in wall co-ordinates; nominal $Re_{\infty r} = 3{\cdot}25 \times 10^5$ ft^{-1}. Unflagged symbols as in figure 6; flagged symbols denote corrected data.

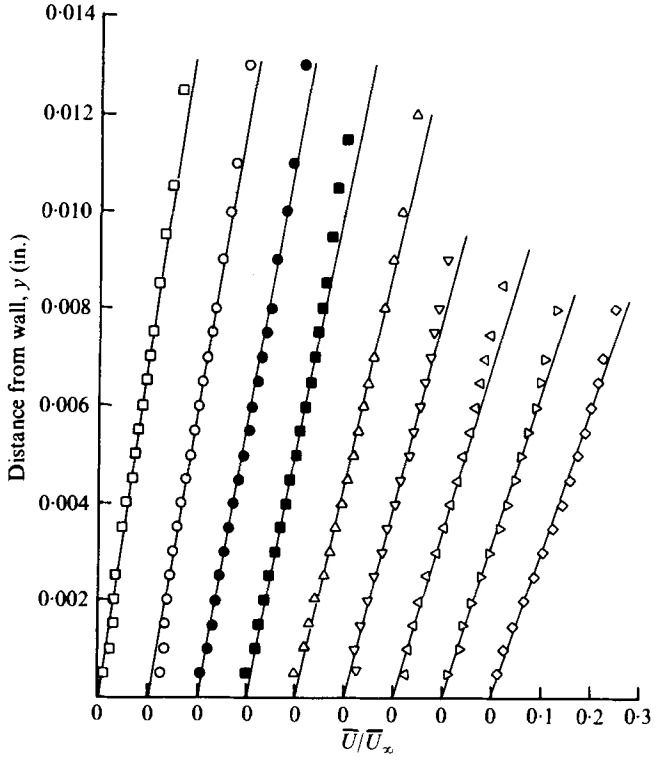

FIGURE 8. Corrected mean velocity profiles close to the wall; nominal $Re_{\infty r} = 3{\cdot}25 \times 10^5$ ft^{-1}. ——, $[d(\overline{U}/\overline{U}_\infty)/dy]_w$ from data on $\bar{c}_f$ from 0·032 in. diameter Preston probe; symbols as in figure 6.

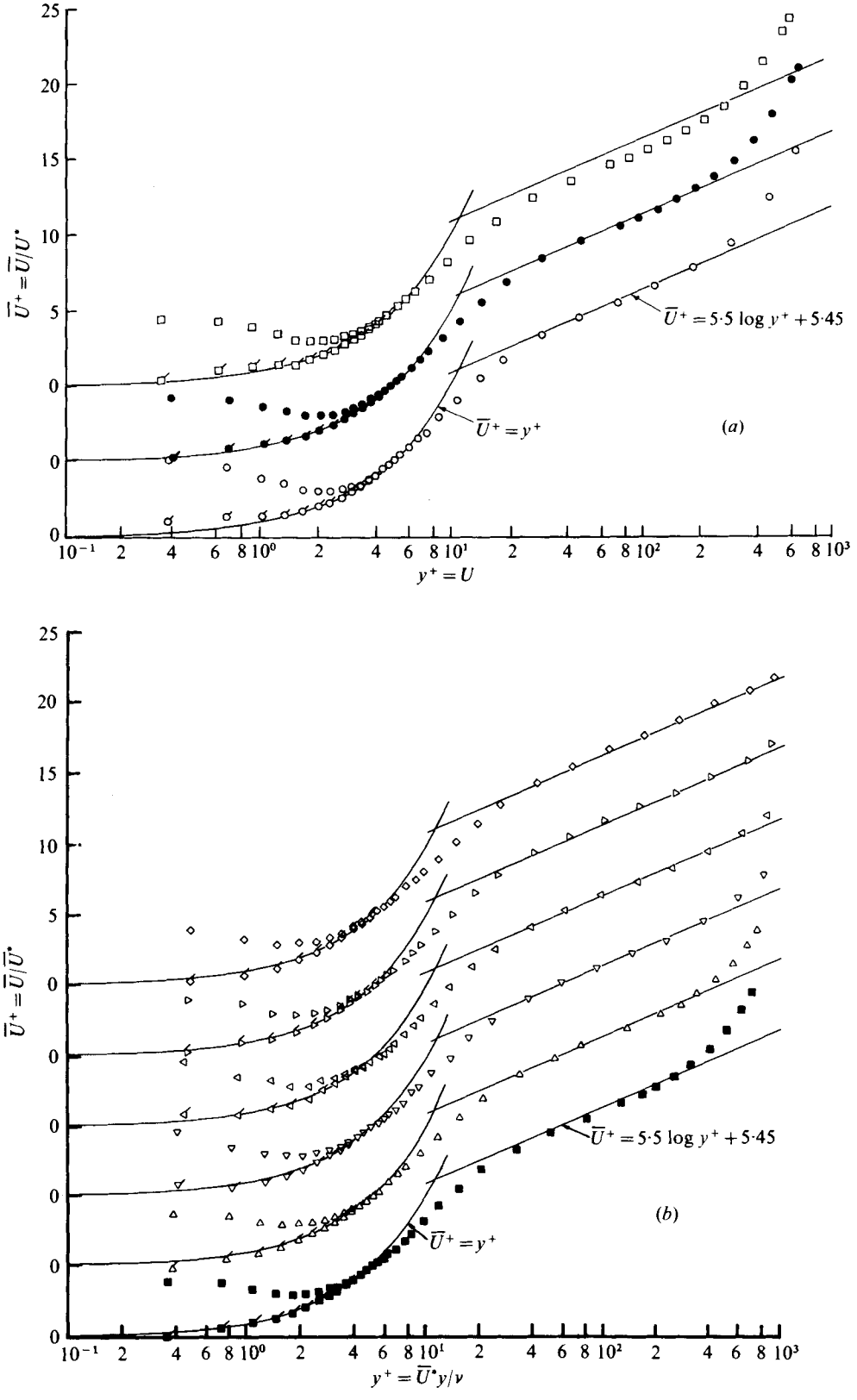

FIGURE 9. Resultant mean velocity profiles in wall co-ordinates; nominal $Re_{\infty r} = 3{\cdot}25 \times 10^5$ ft^{-1}. (*a*) Ports 1, 8 and 9. (*b*) Ports 2–7. Symbols as in figure 7.

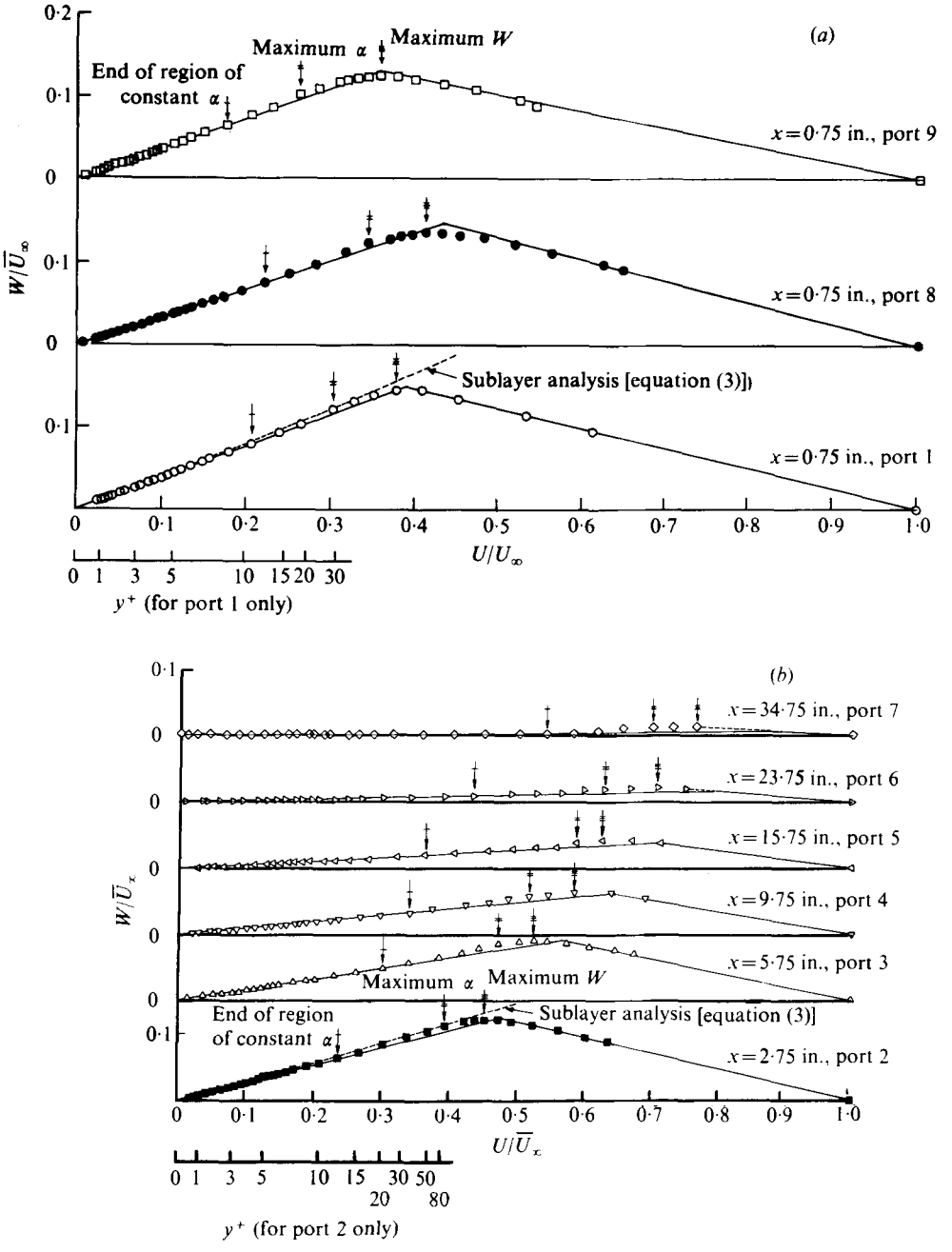

FIGURE 10. Polar plots of mean velocity profile (ports 1, 8 and 9); nominal $Re_{\infty x} = 3{\cdot}25 \times 10^5$ ft^{-1}. (*a*) Ports 1, 8 and 9. (*b*) Ports 2–7.

left-most arrow represents the region of decreasing cross-flow angle. Finally, the small region between the leftmost arrow and the origin represents the region of collateral flow (constant cross-flow angle). The triangles were constructed by simply drawing a line that passed through the origin and the data points in the collateral region and a mean line that passed through the outermost point and the few available points in the outer region. Excluding profiles at the last three stations, y^+ values for the maximum cross-flow angle varied from 27·1 to 144·8 and those for the maximum cross-flow velocity from 117·8 to 362·3, compared with upper limits of the apex of 16 quoted by Johnston (1960), of 150 quoted by Hornung & Joubert (1963) and of 220 quoted by Swamy (1971). The experimental data were examined (Hebbar 1976; Hebbar & Melnik 1976) in terms of an overall correlation (East & Hoxey 1969) of the triangular model between the magnitude and direction of the wall shear-stress vector and the local free-stream conditions. The triangular cross-flow model correlated the relaxing profile data reasonably well.

4.4. *Analysis of flow field close to the wall*

Experimental polar plots by other investigators (see, for example, Nash & Patel 1972, chap. 7) indicate that the inner region between the wall and the apex of a polar plot can extend as far as one-tenth of the boundary-layer thickness, where ratios of local to free-stream velocity may be as high as 0·7. In most of these plots, the inner region was constructed by drawing a mean line through the origin and a few available data points (as few as two in some cases) near the apex (East & Pierce 1972). Most of the existing data therefore indicate collateral flow in this region, i.e. the mean velocity vector does not change its direction. However, recent measurements by Rogers & Head (1969) and Vermeulen (1971), both using specially designed hot-wire anemometer devices, showed skewed flows almost right down to the wall, the data points closest to the wall corresponding to a resultant velocity ratio (local to free-stream) of about 0·2. The very presence of an unusually large number of data points in the inner region and relatively few points in the outer region makes the polar plots (figures 10*a*, *b*) conspicuous when compared with the experimental data of other investigators. With wall-proximity corrections, the corrected resultant velocity ratios closest to the wall were as low as 0·01. It is, therefore, appropriate to discuss in some detail the nature of the part of the flow field close to the wall corresponding to the inner region of the polar plot and to address the question of the existence of near-wall collateral flow in a three-dimensional turbulent boundary layer.

The existence of a collateral flow field is not predicted either by numerical calculations or by a sublayer analysis of the flow. In fact, numerical calculations by East & Pierce (1972) indicate that the assumption of near-wall collateral flow, as suggested by many experimentalists, may not be correct (Pierce & East 1972). The boundary-layer equations in the neighbourhood of the wall lead to the following relation (Nash & Patel 1972, p. 102):

$$\frac{\partial^2 W}{\partial U^2} = \frac{\mu}{\tau_{wx}^2}\left(\frac{\partial p}{\partial z} - \frac{\tau_{wz}}{\tau_{wx}}\frac{\partial p}{\partial x}\right), \tag{1}$$

where τ_w is the wall shear stress. In a collateral flow field $\partial W/\partial U$ = constant, i.e. $\partial^2 W/\partial U^2 = 0$. Thus (1) implies collateral flow only when the resultant pressure gradient is either zero as in a two-dimensional flow or in the direction of the resultant

y (in.)	y^+	$U/\bar{U}_\infty$	$\Delta\alpha = \alpha - \alpha_w$ (deg): Analysis, equation (2)	$\Delta\alpha = \alpha - \alpha_w$ (deg): Measured value
		Port 1 (x = 0·75 in.)		
0·0015	1·02	0·032	0·23	0
0·0045	3·07	0·069	0·49	0
0·0075	5·11	0·117	0·83	0
0·016	10·90	0·206	1·45	0
0·021	14·31	0·239	1·68	0·25
0·028	19·07	0·265	1·86	0·50
0·044	29·97	0·303	2·12	0·875
		Port 2 (x = 2·75 in.)		
0·001	0·73	0·018	0·11	0
0·004	2·92	0·076	0·45	0
0·007	5·11	0·129	0·76	0
0·0165	12·05	0·236	1·39	0
0·0215	15·70	0·269	1·59	0·125
0·0285	20·81	0·302	1·78	0·375
0·0445	32·49	0·338	1·99	0·625
0·0695	50·74	0·369	2·17	0·75
0·1105	80·67	0·394	2·32	0·875

TABLE 1. Comparison of sublayer analysis with measured change in cross-flow angle.

wall shear stress. In general, it implies a non-collateral flow field. Calling the right-hand side of this equation D and integrating, we obtain

$$\tan\alpha - \tan\alpha_w = DU, \tag{2}$$

where D has dimensions s/ft and may be treated as a local constant (with respect to U) in the neighbourhood of the wall for a given velocity profile; α_w is the wall cross-flow angle. The change $\Delta\alpha = \alpha - \alpha_w$ in the cross-flow angle within the sublayer region may be estimated from (2). Integration of (2) yields

$$W/U_\infty = \tfrac{1}{2}D\bar{U}_\infty(U/\bar{U}_\infty)^2 + \tan\alpha_w\,(U/\bar{U}_\infty), \tag{3}$$

which is a parabolic representation of the polar plot very close to the wall.

With the local pressure gradients estimated from the static pressure distribution, the wall cross-flow angle obtained from the hot-film gauge data and the skin friction obtained from the 0·032 in. diameter Preston probe data, the estimated values of D at ports 1 and 2† were $2{\cdot}4816 \times 10^{-3}$ s/ft and $1{\cdot}9836 \times 10^{-3}$ s/ft, respectively. Some typical values of the change in cross-flow angle $\Delta\alpha$ predicted by the analysis are compared with the experimental data in table 1. The predicted shapes of the polar plots are shown in figures 10 (*a*) and (*b*). Although the analysis is strictly valid only very close to the wall ($y^+ < 5$), the predicted values are shown to higher values of y^+ in order to see the trend and to compare them with the maximum decrease in cross-flow angle

† The estimates of the wall pressure gradients at these port locations were considered to be more accurate and reliable (Hebbar 1976).

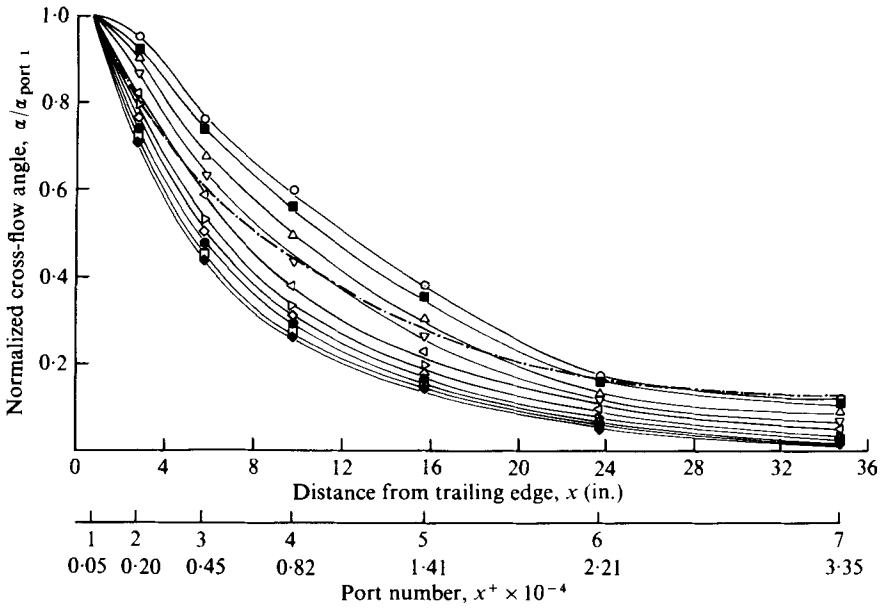

FIGURE 11. Streamwise relaxation (decay) of cross-flow angle in the inner layer at constant y^+ values; nominal $Re_{\infty r} = 3{\cdot}25 \times 10^5$ ft^{-1}. —·—, outer edge of inner layer.

y^+	○ 650	■ 600	△ 500	▽ 400	◁ 300	▷ 200	◇ 150	● 100	□ 50	◆ ≤10

indicated by the hot-wire survey. The analysis predicts the observed trend of the flow field close to the wall, i.e. the unusual behaviour of decreasing cross-flow angle in a narrow region close to the wall. The difference between predicted and experimental results increases with distance from the wall. This is to be expected as the effect of the wall static pressure field decreases with distance from the wall. The overestimation is seen in the predicted profile shapes, which have a slight curvature upwards.

With the above considerations of the near-wall flow field in mind, it is concluded here that, in the absence of the small local transverse pressure gradients close to the wall, the skewing of the relaxing flow could have been much more pronounced practically down to the wall (limited only by the resolution of the sensor), implying a near-wall *non-collateral* flow field consistent with the equations of motion in the neighbourhood of the wall.

4.5. *Relaxation of mean flow*

The polar plots in figures 10 (*a*) and (*b*) show how the three-dimensional flow field returns to a two-dimensional state. In terms of the local free-stream velocity the maximum cross-flow velocity is 14·5% at port 1, less than one-half this value downstream of port 4 and less than one-third downstream of port 5. The polar plot at port 7 is practically a straight line, indicative of a two-dimensional state. Thus the cross-flow decay is relatively fast in the region close to the trailing edge and asymptotic further away from the trailing edge.

A clearer quantitative picture of the relaxation of the mean flow field is conveyed in figure 11, which shows the decay of the normalized cross-flow angle with downstream distance from the trailing edge for various normalized wall distances. For each

wall distance y^+, the cross-flow angle has been normalized by the corresponding cross-flow angle at port 1. Therefore all the graphs start with the same ordinate (unity) at port 1. The dot–dash line shown in the figure represents the outer limit of the inner layer, i.e. the locus of the y^+ values denoting the end of the log region in the law-of-the-wall plots in figures 9 (*a*) and (*b*). With this line as the boundary, it is safe (conservative) to consider the lower half of the graphs ($y^+ \leqslant 200$) as completely representing the inner layer. The upper halves of the graphs ($y^+ > 200$) show mixed regions, all of them representing the outer layer upstream of port 2 but still representing the inner layer downstream of port 6.

Considering the relaxation along the limiting y^+ line for the inner layer (dot–dash line), it is seen that 50 % of the measured decay of the cross-flow takes place in the first 6 in., or nearly 2 boundary-layer thicknesses,† 75 % in the first 14 in., or nearly 4 boundary-layer thicknesses, and 90 % in the first 20 in, or nearly 6 boundary-layer thicknesses. Two significant observations can be made from these graphs: (i) the relaxation of the near flow field based on the decay of the cross-flow is much faster in the inner layer than in the outer layer and (ii) the relaxation is almost complete after a streamwise distance of approximately 10 boundary-layer thicknesses.

4.6. *Relaxation of wall shear-stress vector*

Figure 12 shows the local limiting streamline angle (measured from the local horizon) and the resultant mean skin-friction coefficient $\bar{c}_f$ determined from the wall shear-stress measurements in the relaxing region behind the trailing edge of the hump. Also shown for comparison are the wall cross-flow angles extrapolated from the hot-wire direction profiles at the respective port locations and the value of $\bar{c}_f$ estimated from the resultant mean velocity profile data using Bradshaw's simplified version of Clauser's technique (Hebbar 1976; Hebbar & Melnik 1976). In addition, the data from the wall shear-stress measurements in the two-dimensional boundary layer (in the absence of the hump) are included. The nature of the agreement among different measurement techniques attests to the consistency (within experimental precision) of the experimental data from various probes. The ensuing discussion on the relaxation of the wall shear-stress vector behind the trailing edge of the hump is based on the direction of the limiting streamline indicated by the hot-film gauge and the skin-friction coefficient indicated by the 0·032 in. diameter Preston probe.

The limiting streamline angle decays rapidly in the region close to the trailing edge, but the rate of decay decreases with downstream distance. The skin-friction coefficient increases rapidly in the region close to the trailing edge, the rate of increase decreasing with downstream distance. Taking the difference between the measured values at ports 1 and 7 as the total relaxation (decay of α_w and increase of $\bar{c}_f$) in the streamwise distance of 34 in. between these ports, the following observations may be made:

(i) 50 % of the relaxation of the direction of the mean wall shear-stress vector occurs in the first 4 in., or a little more than one boundary-layer thickness, 75 % within the

† The existing limited experimental data on relaxation studies and the choice of relaxation scale used in these studies have been commented upon in Hebbar (1976). Although the boundary-layer thickness may not be an appropriate length scale for the inner layer, it is used here so that the relaxation of the inner layer can be compared with that of the adjacent portion of the outer layer covered by the hot-wire surveys. The non-dimensionalized streamwise distance x^+ of each port location, based on the length scale $\nu/\bar{U}^*$, is also included in figure 11.

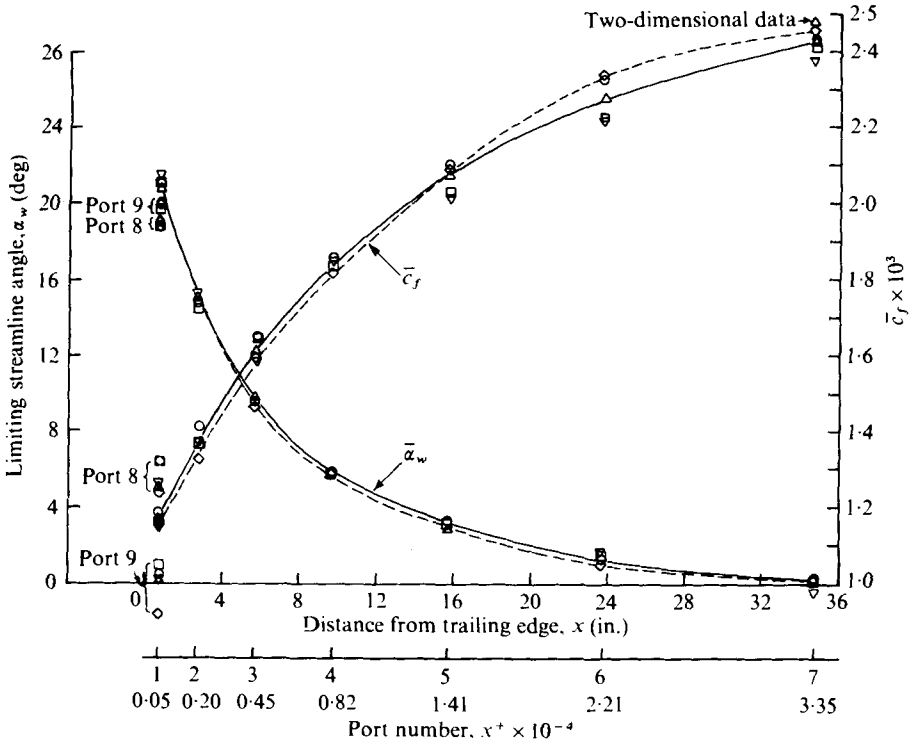

FIGURE 12. Distribution of limiting streamline angle (wall cross-flow angle) and resultant mean skin-friction coefficient in the relaxing boundary layer; nominal $Re_{\infty r} = 3{\cdot}25 \times 10^5$ ft^{-1}. —○—, hot-film gauge, α_w; ○, hot-film gauge, $\bar{c}_f$; □, sublayer fence; △, 0·032 in. diameter Preston probe, α_w; —△—, 0·032 in. diameter Preston probe, $\bar{c}_f$; ▽, 0·018 in. diameter Preston probe; --◇--, α_w from hot-wire extrapolation or $\bar{c}_f$ from velocity profile.

first 10 in., or nearly three boundary-layer thicknesses, and 90 % within the first 19 in., or nearly 5½ boundary-layer thicknesses. The corresponding relaxation of the magnitude of the resultant wall shear stress occurs within 2½, 5 and 7½ boundary-layer thicknesses, respectively.

(ii) The mean wall shear-stress vector almost relaxes (in both direction and magnitude) to a two-dimensional state in approximately 10 boundary-layer thicknesses.

4.7. *Turbulence profiles in the relaxing region*

The three-dimensional turbulence data deduced from the hot-wire surveys are shown in figures 13 and 14. The profiles in figure 13 show, in wall co-ordinates, the turbulence distribution in the inner layer at selected locations of the relaxing region. The root-mean-square values $(\overline{u_1^2})^{\frac{1}{2}}$ and $(\overline{w_1^2})^{\frac{1}{2}}$ of the longitudinal and lateral turbulence, in the local co-ordinate system (x_1, y_1, z_1), have been non-dimensionalized by the local skin-friction velocity $\bar{U}^*$, and their correlation $\overline{u_1 w_1}$ by the square of $\bar{U}^*$. Here x_1 is parallel to the local mean velocity vector $\bar{U}$, z_1 is normal to x_1 in the plane parallel to the wall and y_1 is perpendicular to x_1 and z_1 (see figure 2). Also shown for comparison in each of these figures is the corresponding two-dimensional profile at port 7 (considered representative of the asymptotic state of the relaxing turbulence field).

The point of interest in figure 13(*a*) is the magnitude and location of the peaks of

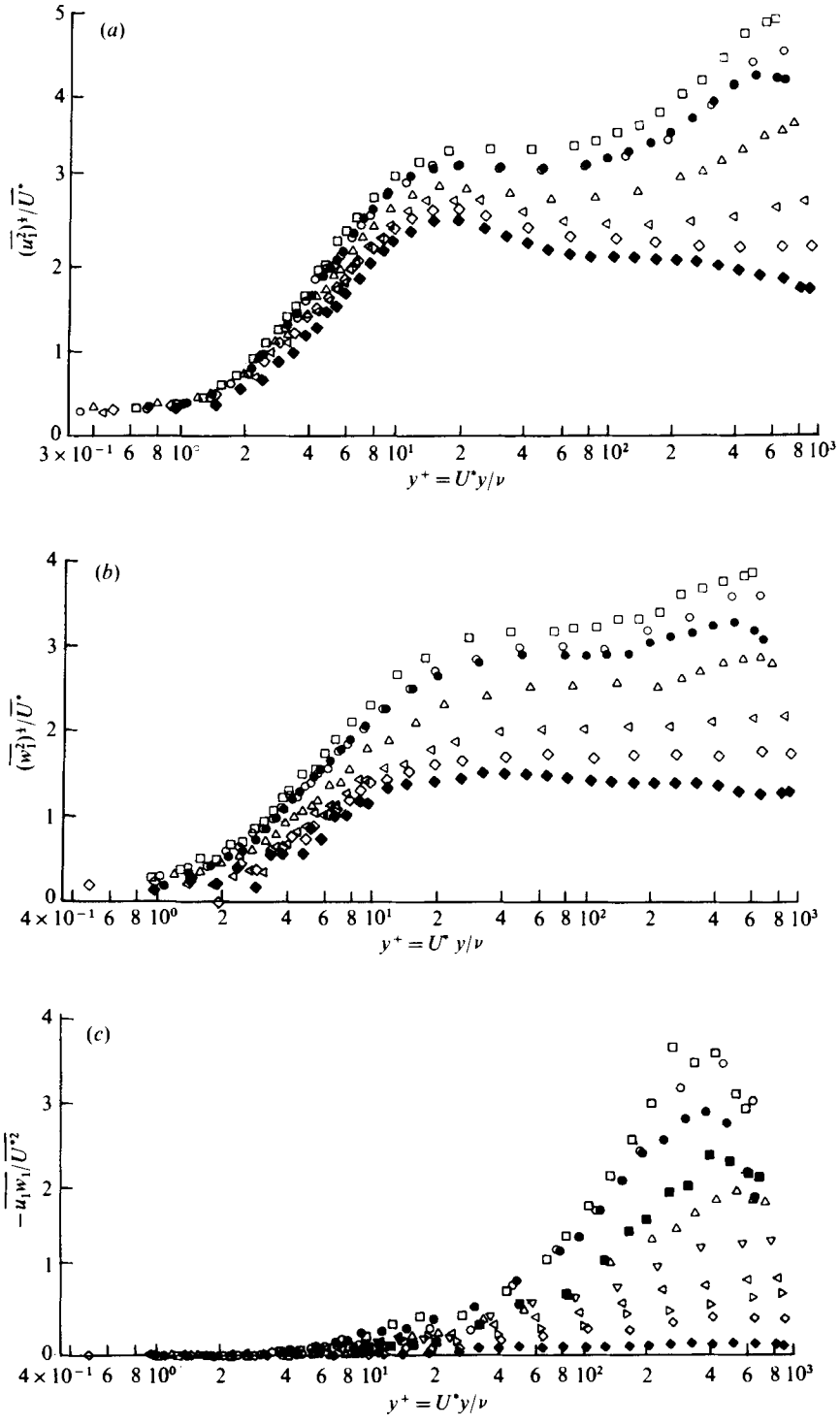

FIGURE 13. (*a*) Longitudinal turbulence, (*b*) lateral turbulence and (*c*) $-\overline{u_1 w_1}$ correlation data in wall co-ordinates; nominal $Re_{\infty r} = 3{\cdot}25 \times 10^5$ ft^{-1}. Symbols as in figure 6.

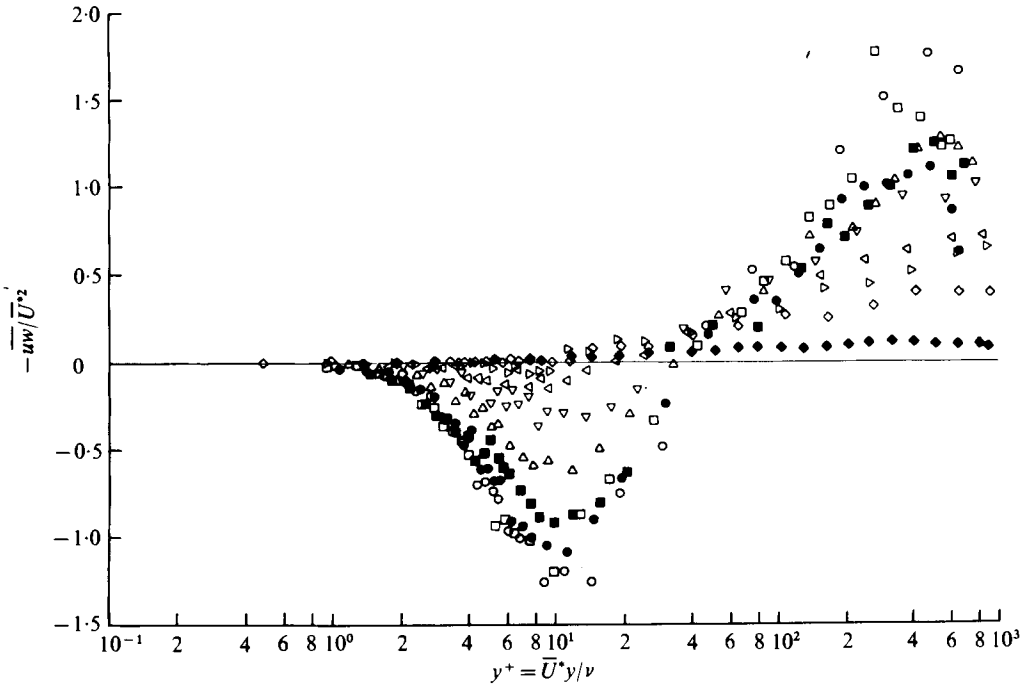

FIGURE 14. $-\overline{uw}$ correlation data in wall co-ordinates; nominal $Re_{\infty r} = 3{\cdot}25 \times 10^{5}$ ft^{-1}. Symbols as in figure 6.

the longitudinal turbulence intensity in the relaxing field relative to the two-dimensional data. Although no quantitative conclusion can be drawn, the increase and shift (away from the wall) in the peaks are clearly seen at all port locations, the effects being more pronounced in the region very close to the trailing edge. This is not surprising in view of the fact that the mean velocity profiles shown in figure 6, particularly those close to the trailing edge, resemble those in two-dimensional flows with an adverse pressure gradient, where similar effects on turbulent fluctuations have been noticed (Schubauer & Klebanoff 1951). Similar trends are noticeable also in the distribution of lateral turbulence intensity in figure 13 (*b*). More significant in three-dimensional flows is the presence of the $\overline{u_1 w_1}$ correlation (figure 13*c*) in the relaxing boundary layer, particularly close to the trailing edge.

The outward shift in the peaks in regions close to the trailing edge is very pronounced and appears to extend into the outer region of the boundary layer. Moreover, in these regions, the maximum values are attained gradually and the peak characteristic of a two-dimensional flow disappears. The maximum values are exhibited by the turbulence data at port 9 (see table 2), which is expected from the nature of the mean velocity profile at that location (figure 6). There does not appear to be any similarity region close to the wall corresponding to that which the Prandtl hypothesis predicts for two-dimensional flows (Laufer 1950).

Because the cross-flow angle α is small ($\alpha_{\max} = 21{\cdot}875°$), the longitudinal and lateral turbulence intensities $(\overline{u^2})^{\frac{1}{2}}$ and $(\overline{w^2})^{\frac{1}{2}}$ in the reference co-ordinate system (x, y, z) (figure 2) do not differ appreciably from $(\overline{u_1^2})^{\frac{1}{2}}$ and $(\overline{w_1^2})^{\frac{1}{2}}$, respectively. The general trends of variation of $(\overline{u^2})^{\frac{1}{2}}$ and $(\overline{w^2})^{\frac{1}{2}}$ in the inner layer follow those of $(\overline{u_1^2})^{\frac{1}{2}}$ and $(\overline{w_1^2})^{\frac{1}{2}}$, respec-

	Port 9	Port 7 (two-dimensional)
Longitudinal turbulence, $(\overline{u_1^2})^{\frac{1}{2}}/\overline{U}^*$	5·00	2·5
Lateral turbulence, $(\overline{w_1^2})^{\frac{1}{2}}/\overline{U}^*$	3·79	1·50
Cross correlation, $-\overline{u_1 w_1}/\overline{U}^{*2}$	1·77	$<0{\cdot}12$

TABLE 2. Maximum values of turbulence fluctuations in wall co-ordinates.

tively; therefore they have not been presented graphically. But the variation of the cross-correlation $-\overline{uw}$ in the inner layer is significantly different, both in magnitude and direction, from that of $-\overline{u_1 w_1}$ discussed earlier. Figure 14 shows the variation of $-\overline{uw}$ in wall co-ordinates.The most striking feature here is the sign reversal of the correlation as the wall is approached. The y^+ value corresponding to zero cross-correlation increases with decreasing $\overline{U}^*$, the maximum y^+ value being 40, at port 9. In other words, close to the trailing edge the sign reversal occurs at greater distances from the wall. It is strongly suspected that the sign reversal is caused by the presence of the slight adverse pressure gradient in the transverse direction that was observed in the spanwise wall static pressure data.

4.8. *Relaxation of turbulence*

Compared with the mean flow field discussed earlier, the turbulence field relaxes more slowly as can be seen by comparing the three-dimensional and two-dimensional turbulence data at the most downstream port location (port 7) in figure 15, where the maximum turbulence fluctuations in the boundary layer are plotted against downstream distance. All the fluctuations have been non-dimensionalized by the respective fluctuations at port 1. The rate of decrease of the maximum turbulence is rapid in the region close to the trailing edge, but decreases with downstream distance. The measured maximum values at the last port are higher than the corresponding two-dimensional values by 11·16 % for $(\overline{u_1^2})^{\frac{1}{2}}$ and 21·30 % for $(\overline{w_1^2})^{\frac{1}{2}}$. Taking the difference between the measured maximum values at ports 1 and 7 as the total relaxation (decay) of turbulence in the streamwise distance of 34 in. between these ports, the following observations may be made.

(i) 50 % of the relaxation in $(\overline{u_1^2})^{\frac{1}{2}}_{\max}$ ($(\overline{w_1^2})^{\frac{1}{2}}_{\max}$, $(-\overline{u_1 w_1})_{\max}$) occurs in the first 6·25 in. (9 in., 6·75 in.), or nearly 2 (2·5, 2) boundary-layer thicknesses, 75 % in the first 13·25 in. (18·5 in., 15·75 in.), or nearly 4 (5·5, 4·5) boundary-layer thicknesses, and 90 % in the first 22·25 in. (25 in., 24·25 in.), or nearly 6·5 (7, 7) boundary-layer thicknesses.

(ii) Compared with the streamwise relaxation of the mean flow, the relaxation of the turbulence intensities is slower and is not complete after 10 boundary-layer thicknesses. This relaxation length may be compared with the observations of Bissonette (1974), where the 'history' of the turbulence seems to persist for more than 20 boundary-layer thicknesses.

4.9. *Spanwise variations in the flow field*

Some spanwise variations were expected because of the low aspect ratio of the hump. Even the nominally two-dimensional boundary layer upstream of the hump was contaminated by transverse non-uniformities which would be amplified in flowing over the hump (Winkelmann 1976). However, these variations should not preclude

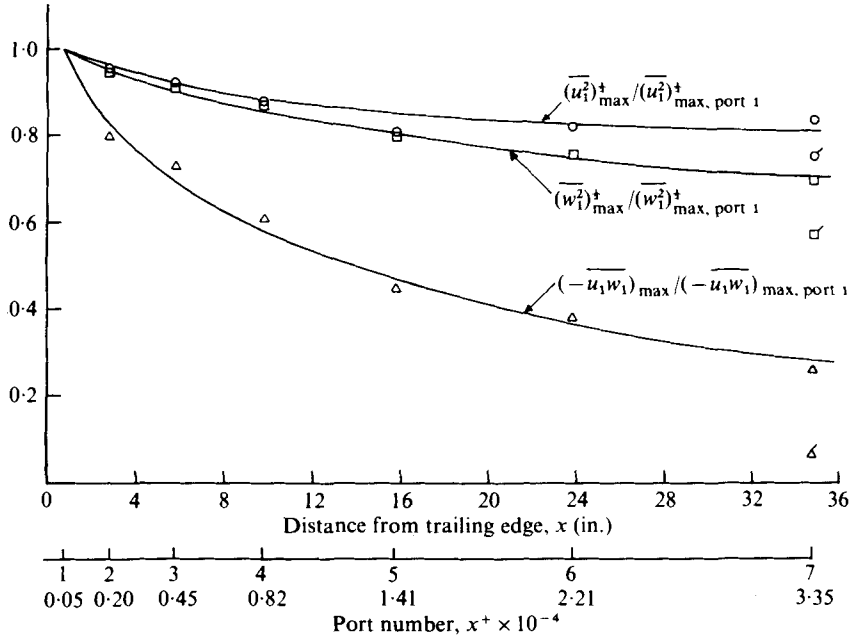

FIGURE 15. Streamwise relaxation (decay) of maximum turbulence fluctuations measured during partial hot-wire surveys; nominal $Re_{\infty r} = 3{\cdot}25 \times 10^5$ ft^{-1}. Flagged symbols denote two-dimensional values.

an interpretation of the local three-dimensional flow phenomenon based on local measurements. An assessment of the spanwise variations in the relaxing flow field appears in Hebbar (1976). Only typical values will be quoted here. Considered over a span of 15 in. between ports 8 and 9, the maximum spanwise variation in the measured resultant mean velocity was nearly 10 % of the local free-stream velocity and the maximum spanwise variation in the cross-flow angle was less than 2·5°. These variations may be expected to be considerably smaller over a restricted span of, say, 7 in., or approximately one boundary-layer thickness, on either side of the streamwise line of instrumentation ports. Over the same restricted span, it was estimated that the spanwise variation in the direction and the magnitude of the wall shear stress did not exceed 1° and 10 %, respectively. The spanwise variations in the turbulent fluctuations considered over the same span may be expected to be not more than 5 % in $(\overline{u_1^2})^{\frac{1}{2}}_{max}$, 7 % in $(\overline{w_1^2})^{\frac{1}{2}}_{max}$ and 12 % in $(-\overline{u_1w_1})_{max}$.

5. Conclusions

The data from the three-dimensional wall and near-wall measurements were analysed with particular emphasis on the nature of the mean flow field very close to the wall and the streamwise relaxation characteristics of the mean flow and some turbulence quantities. The important findings of the present study are summarized below.

(i) *Wall-proximity corrections.* The experimental data indicated that the apparent dimensionless velocity profiles in the viscous sublayer are universal (local) and that the wall influence on hot-wire readings is negligible beyond $y^+ = 5$.

(ii) *Mean direction profiles.* The experimental mean direction profiles exhibited the usual features characteristic of a simple cross-flow profile but with a relatively smaller collateral region adjacent to the wall (the smallest extending up to $y^+ = 9{\cdot}7$). The unusual feature of these profiles was the presence of a narrow region of slightly decreasing cross-flow angle (1° or less) that extended from the point of maximum cross-flow angle down to the outer limit of the collateral region. On the basis of a sub-layer analysis of the flow field, it is concluded that, in the absence of the small local transverse adverse pressure gradients close to the wall, the skewing of the flow could have been much more pronounced practically down to the wall (limited only by the resolution of the sensor), implying a near-wall *non-collateral* flow field consistent with the equations of motion in the neighbourhood of the wall.

(iii) *Wall similarity region.* The existence of wall similarity in the relaxing flow field was confirmed in the form of a log law based on the resultant mean velocity and resultant friction velocity (obtained from the measured skin friction).

(iv) *Turbulence data.* The three-dimensional turbulence profiles do not appear to indicate any similarity region close to the wall like that which the Prandtl hypothesis predicts for two-dimensional flows. Compared with the two-dimensional peak values, the maximum longitudinal turbulence intensity $(\overline{u_1^2})^{\frac{1}{2}}/\overline{U}^*$ is doubled and the maximum lateral turbulence intensity $(\overline{w_1^2})^{\frac{1}{2}}/\overline{U}^*$ is increased by a factor of $1\frac{1}{2}$–2. But the maximum values are attained gradually and the sharp peak characteristic of a two-dimensional flow disappears.

(v) *Streamwise relaxation.* The streamwise relaxation of the mean flow field (the cross-flow angle) is much faster in the inner layer than in the outer layer. The relaxation of the mean flow in the inner layer is almost complete after approximately 10 boundary-layer thicknesses. The wall shear-stress vector almost relaxes to a two-dimensional state in approximately the same distance. However, the relaxation of turbulence is slower and is not complete after 10 boundary-layer thicknesses.

The work reported herein is based on the Ph.D. dissertation of the first author and was performed at the University of Maryland with partial financial support from NASA, the Office of Naval Research and the Minta Martin Fund for Aeronautical Research. The authors gratefully acknowledge the unstinting efforts of Dr Allen E. Winkelmann, which were instrumental to the accomplishment of these experiments.

REFERENCES

Berg, B. van den, Elsenaar, A., Lindhout, J. P. F. & Wesseling, P. 1975 *J. Fluid Mech.* **70**, 127.

Bissonnette, L. R. 1974 *J. Fluid Mech.* **63**, 369.

Bradshaw, P. 1969 Outlook for three-dimensional procedures. In *Proc. Computation of Turbulent Boundary Layers:* 1968 *AFOSR-IFP-Stanford Conf.*, vol. 1, p. 427.

Bradshaw, P. 1971 *J. Fluid Mech.* **46**, 417.

Bradshaw, P. & Terrell, M. 1969 *Nat. Phys. Lab. Aero. Rep.* no. 1305.

Cebeci, T. 1974 *A.I.A.A. J.* **12**, 779.

Cebeci, T. 1975 *A.I.A.A. J.* **13**, 1056.

East, L. F. & Hoxey, R. P. 1969 *Aero. Res. Counc. R. & M.* no. 3653.

East, J. L. & Pierce, F. J. 1972 *A.I.A.A. J.* **10**, 1216.

Etheridge, D. W. 1972 Three-dimensional turbulent boundary layers on a 45° swept plate and drag calculation for a series of bodies of revolution. Ph.D. thesis, University of London.

HEBBAR, K. S. 1976 An experimental investigation of the near-wall region of a three-dimensional incompressible turbulent boundary layer relaxing in a zero pressure gradient. Ph.D. dissertation, University of Maryland (University Microfilms no. 77-9513).

HEBBAR, K. S. & MELNIK, W. L. 1976 Measurements in the near-wall region of a relaxing three-dimensional low speed turbulent air boundary layer. *Dept. Aerospace Engng, Univ. Maryland Tech. Rep.* no. AE-76-1.

HORNUNG, H. G. & JOUBERT, P. N. 1963 *J. Fluid Mech.* **15**, 368.

JOHNSTON, J. P. 1960 *J. Basic Engng, Trans. A.S.M.E.* D **82**, 233, 622.

JOHNSTON, J. P. 1970 *J. Fluid Mech.* **42**, 823.

KLINKSIEK, W. F. & PIERCE, F. J. 1970 *J. Basic Engng, Trans. A.S.M.E.* D **92**, 83.

LAUFER, J. 1950 *N.A.C.A. Tech. Note* no. 2123.

MELLOR, G. L. 1967 *A.I.A.A. J.* **5**, 1570.

NASH, J. F. 1969 *J. Fluid Mech.* **37**, 625.

NASH, J. F. & PATEL, V. C. 1972 *Three-Dimensional Turbulent Boundary Layers.* Atlanta: SBC Technical Books.

OKA, S. & KOSTIC, Z. 1972 Influence of wall proximity on hot-wire velocity measurements. *DISA Inf.* no. 13, p. 29.

PATEL, V. C. 1965 *J. Fluid Mech.* **23**, 185.

PIERCE, F. J. & EAST, J. L. 1972 *A.I.A.A. J.* **10**, 334.

POWER, J. L. 1973 Wall shear stress and mean-velocity measurements in a three-dimensional turbulent boundary layer. *NSRDC Rep.* no. 4056.

PRAHLAD, T. S. 1968 *A.I.A.A. J.* **6**, 1772.

PRAHLAD, T. S. 1973 *A.I.A.A. J.* **11**, 359.

ROGERS, B. K. & HEAD, M. R. 1969 *Aero. J. Roy. Aero. Soc.* **73**, 796.

ROSE, W. G. 1962 *A.S.M.E. Symp. Measurement in Unsteady Flow*, p. 85.

SCHUBAUER, G. B. & KLEBANOFF, P. S. 1951 *N.A.C.A. Rep.* no. 1030, p. 689.

SWAMY, N. V. C. 1971 *Z. Flugwiss.* **19**, 496.

VERMEULEN, A. J. 1971 Measurements of three-dimensional turbulent boundary layers. Ph.D. dissertation, University of Cambridge.

WHEELER, A. J. & JOHNSTON, J. P. 1973 *J. Fluids Engng, Trans. A.S.M.E.* I **95**, 415.

WILLS, J. A. B. 1967 *Nat. Phys. Lab. Aero. Rep.* no. 1251.

WINKELMANN, A. E. 1976 Experimental studies of a two and a three-dimensional low speed turbulent boundary layer. Ph.D. dissertation, University of Maryland (University Microfilms no. 77–26552).